scientific reports

Check for updates

OPEN

Nonlinear radiative Maxwell nanofluid flow in a Darcy–Forchheimer permeable media over a stretching cylinder with chemical reaction and bioconvection

Chunyan Liu[1,2], Muhammad Usman Khan[3], Muhammad Ramzan[1,3], Yu-Ming Chu[4,5]✉, Seifedine Kadry[6], M. Y. Malik[7] & Ronnason Chinram[8]

Studies accentuating nanomaterials suspensions and flow traits in the view of their applications are the focus of the present study. Especially, the usage of such materials in biomedical rheological models has achieved great importance. The nanofluids' role is essential in the cooling of small electronic gizmos like microchips and akin devices. Having such exciting and practical applications of nanofluids our goal is to scrutinize the Maxwell MHD nanofluid flow over an extended cylinder with nonlinear thermal radiation amalgamated with chemical reaction in a Darcy–Forchheimer spongy media. The presence of gyrotactic microorganisms is engaged to stabilize the nanoparticles in the fluid. The partial slip condition is considered at the boundary of the stretching cylinder. The Buongiorno nanofluid model is betrothed with impacts of the Brownian motion and thermophoresis. The analysis of entropy generation is also added to the problem. The highly nonlinear system is tackled numerically is addressed by the bvp4c built-in function of the MATLAB procedure. The outcomes of the prominent parameters versus embroiled profiles are portrayed and conversed deeming their physical significance. It is perceived that fluid temperature is augmented for large estimates of the radiation and Darcy parameters. Moreover, it is noticed that the magnetic and wall roughness parameters lower the fluid velocity. To corroborate the presented results, a comparison of the current study with a previously published paper is also executed. An outstanding correlation in this regard is attained.

List of symbols

B_0	Magnetic field intensity
B_1	Wall roughness parameter
B_2	Wall thermal parameter
B_3	Concentration slip parameter
B_4	Motile slip parameter
Br	Brinkman number

[1]School of Science, Beijing University of Civil Engineering and Architecture, Beijing 100044, People's Republic of China. [2]Beijing Key Laboratory of Functional Materials for Building Structure and Environment Remediation, Beijing University of Civil Engineering and Architecture, Beijing 100044, People's Republic of China. [3]Department of Computer Science, Bahria University, Islamabad 44000, Pakistan. [4]Department of Mathematics, Huzhou University, Huzhou 313000, People's Republic of China. [5]Hunan Provincial Key Laboratory of Mathematical Modeling and Analysis in Engineering, Changsha University of Science and Technology, Changsha 410114, People's Republic of China. [6]Faculty of Applied Computing and Technology, Noroff University College, Kristiansand, Norway. [7]Department of Mathematics, College of Sciences, King Khalid University, Abha 61413, Kingdom of Saudi Arabia. [8]Division of Computational Science, Faculty of Science, Prince of Songkla University, Hat Yai, Songkhla 90110, Thailand. ✉email: chuyuming@zjhu.edu.cn

D_T Thermophoretic diffusion coefficient (m^2/s)
c_b Capacity
C_{f_x} Drag force coefficients
k_2 Permeability of porous medium
C_w Wall's concentration
D_B Brownian diffusion coefficient (m^2/s)
C_∞ Ambient liquid concentration
C Liquid concentration ($kg\,m^{-3}$)
c_p Heat Specific capacity ($J\,kg^{-1}\ k^{-1}$)
D_n Diffusivity of the microorganism (m^2/s)
Pe Peclet numbers
F Non-uniform inertial coefficient
Fr Forchheimer number
L_4 Motile slip coefficient
l Characteristic length (m)
j_w Mass flux (m/s)
Lb Bioconvection Lewis number
K Magnetic interaction parameter
L_2 Thermal slip coefficient
k^* Mean absorption coefficient $\left({}^{1}/_{\mathrm{m}}\right)$
q_n Surface motile microorganisms (W/m^2K)
Nb Brownian motion parameters
u_0 Reference velocity (m/s)
n Reaction order
k Thermal conductivity $\left({}^{\mathrm{W}}/_{\mathrm{m}}\right)$
L_1 Velocity slip coefficient
N_G Rate of Entropy generation
L_3 Concentration slip coefficient
Nu_x Local Nusselt number
M Curvature parameter $\left(m^{-1}\right)$
q_w Wall heats (W/m^2)
Nt Thermophoresis parameter
Pr Prandtl number
q_r Radiation heat flux (W/m^2)
Nn_x Density number of motile microorganisms
r Radial coordinate (m)
Rd Radiation parameter
T_w Wall's temperature (K)
σ_1 Electrical conductivity $\left({}^{\mathrm{S}}/_{\mathrm{m}}\right)$
u Velocity component along x-direction (m/s)
Sc Schmidt number
L Diffusion parameter
T_∞ Ambient fluid temperature (K)
σ^* Stefan–Boltzmann constant $\left({}^{\mathrm{W}}/_{\mathrm{m}^2\mathrm{K}^4}\right)$
w_c Constant all-out cell swimming speed (m/s)
S_G Entropy generation
σ Bioconvection parameter
ΔT Temperature difference
Sh_x Local Sherwood number
v Velocity component along r-direction (m/s)
x Axial coordinate (m)
u_w Stretching velocity (m/s)

Greek symbols
α Thermal diffusivity (m^2/s)
α_1 Temperature difference parameter
α_2 Concentration difference parameter
α_3 Motile difference parameter
β Deborah number in terms of velocity time
γ Chemical reaction parameter
λ Porosity parameter
λ_1 Reaction rate
λ^* Relaxation time
ν Kinematic viscosity (m^2/s)
ρ Density (kg/m^3)
μ Absolute viscosity (Pa/s)

η Similarity variable
ψ Stream function (m^2/s)
θ_w Temperature ratio parameter
τ The quotient of the effective heat capacity of the nano-particle material and of the fluid

Subscripts
∞ Condition at the infinity
w Condition at the wall

Nanofluid, an arising field of engineering, has caught the eye of numerous researchers who were observing the ways to improve the efficiency of cooling measures in industries. Nanofluids are used to improve rates of heat transfer in an assortment of applications including nuclear reactors, transportation industry, mechanical cooling applications, heat exchangers, micro-electromechanical systems, fiber, and granular insulation, chemical catalytic reactors, packed blood flow in the cardiovascular system engaging the Navier–Stokes equation. Advanced thermal features of the nanofluid are imperative in many fields like pharmaceutical, air-conditioning, micromanufacturing, microelectronics, power generation, thermal therapy for cancer surgery, transportation, chemical, and metallurgical engineering fields, etc. Due to the significant advancement in aerodynamics automotive, there is great importance in breaking down systems by direct heat dissipation. Many investigators have recently added some work to promote solar cells with high digestion of solar radiation. As Choi and Eastman[1] found that the incorporation of nanoparticles to the base liquids significantly enhances their thermal efficiency. The rising demand for highly efficient cooling devices encourages Koo and Kleinstreuer[2] to study the steady laminar nanofluid flow in micro heat sinks. It is noticed that very low nanoparticle concentration in nanofluids results in a higher thermal conductivity that exhibits a remarkable state of nanofluids[3,4]. Bilal et. al[5] scrutinized the numerical study of unsteady Maxwell flow of nanofluid influenced by the magnetic field, melting heat, and the Fourier and Fick laws. This investigation reveals that the liquid temperature is dropped for versus melting heat and unsteadiness parameters. The flow of 3D non-radiative Maxwell nanofluid with thermal and solutal stratification with chemical reaction is analytically studied by Tlili et. al[6]. Here, the noticeable outcome of the model is that the fluid concentration and temperature are declined for solutal and thermal stratifications respectively. Farooq et al.[7] analytically conversed the Maxwell nanofluid flow over an exponentially extended surface. Various researchers revealed the numerous aspects of the Williamson nano liquid[7–22].

The term Darcy–Forchheimer comes from the law of Darcy which interprets the liquid flow along a spongy channel. This law was originated and dependent upon the consequences of analysis on the water flow across the beds of sand. Movements in the spongy medium in which inertial effects are prominent come with the variations of Reynolds numbers. Therefore, this introductory term is adding up to the Darcy equation and is referred to as the Darcy–Forchheimer term. This term represents the non-linear behavior of the flow data versus pressure difference. With wide utilization of grain stockpiling, petroleum technology, frameworks of groundwater and oil assets, this Darcy law is of immense importance in the field of Fluid Mechanics. In places where the porous medium has larger flow rates due to non-uniformity, such as near the wall, Darcy's law is not applicable. The substance with stomata is named as a permeable medium. It includes an application of large numbers such that oil manufacturing, liquid flow in catalytic vessels, and reservoirs, etc. The suggestion of the fluid flow passes a porous surface was first given by Darcy[23] in 1856. However, this idea couldn't be so famous inferable from its restrictions of lower porosity and smaller speed. Afterward, Forchheimer[24] amended the equation of momentum by adding the square velocity condition into the Darcian velocity to convey the undeniable lack. Muskat[25] later call it the "Forchheimer term" which is true of the high Reynolds number. Pal and Mondal[26] addressed the Darcy–Forchheimer model over permeable media past the linearly expanded region and assume that concentration distribution is diminishing function of the electric field parameter. The movement of the hydromagnetic nano liquid past the Darcy–Forchheimer media forum effect on the boundary condition of second order is mathematically evaluated by Ganesh et al.[27]. Alshomrani et al.[28] explained the 3D Darcy–Forchheimer law with carbon nanotubes and homogeneous heterogeneous reactions. The viscous nanofluid with Darcy–Forchheimer effect over a curved area is analyzed by Saif et al.[29]. Seth et al.[30] examined mathematically the movement of carbon nanotubes over a porous Darcy–Forchheimer media in a rotating frame and many therein[31–41].

In numerous processes including dispersion of nutrients in nerves, condensation in mixtures, and thermal insulation, mass transfer plays a vital role. One live example of transfer of mass may be seen in the living matter processes like respiration and sweating. A good number of studies may be quoted where chemical reactions play a vital role in mass transfer procedures.

Recently, Mahmood[42] explored the nanofluid flow with an amalgamation of the CNT's of both types and the engine oil over a stretched surface with the impact of the activation energy merged with the chemical reaction. The problem is solved numerically and with a surface response statistical technique. It is inferred from this model that the surface drag coefficient is negatively sensitive concerning the magnetic parameter. The numerical solution of the nanofluid flow involving the CNT's and water over an extended/contracting sheet with quartic autocatalysis chemical reaction and Thompson and Troian slip boundary conditions is discussed by Ramzan et al.[43]. The results exposed that the fluid concentration is enhanced for quartic autocatalysis chemical reaction. Khan et al.[44] numerically tackled the Carreau nanofluid flow over an extended surface in a Homann stagnation region with chemical reaction and modified Fourier law using shooting scheme. The study divulges that the fluid velocity hinders owing to the Hartmann number and the porosity parameter. In the perspective of its clarity, the remarkable work of current researchers, see few studies[45–56].

In thermodynamics, entropy is an essential concept. One of the most powerful methods for investigating the efficiency of thermal systems is entropy generation analysis. The idea of irreversibility is inextricably related to

Authors	Buongiorno model	Maxwell nanofluid flow over a cylinder	Darcy–Forchheimer impact	Nonlinear thermal radiation	Bioconve-ction	Chemical reaction
Islam et al.[15]	√	√	×	×	×	×
Ahmed et al.[16]	√	√	×	√	×	×
Hayat et al.[66]	√	√	×	×	×	√
Raju et al.[67]	√	√	×	×	×	×
Present	√	√	√	√	√	√

Table 1. A literature analysis for the individuality of the stated model. (√) means said effect present, and (×) signifies the impact is absent.

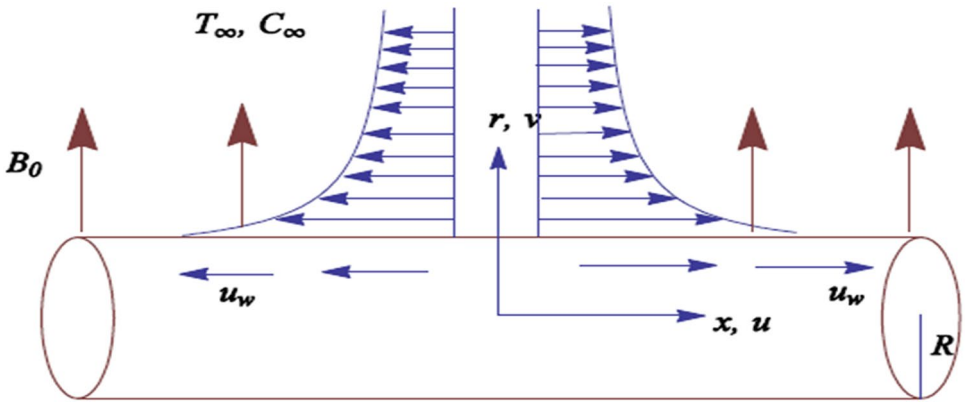

Figure 1. The geometry of the flow.

the concept of entropy. All have an instinctive understanding of irreversibility. For example, by playing a video game in both forward and reverse, we can merely explain the irreversibility phenomenon by using backward order. There are numerous forward procedures of daily life that cannot be undone, such as pouring water into a bottle, egg unscrambling, unconstrained expansion of fluids, plastic deformation, gas uprising from the chimney, etc. In this perspective, Yusuf et al.[57] explored the entropy generation in a Maxwell fluid flow over an inclined extended surface in a non-Darcian spongy media with thermal radiation. An analytical solution of the erected mathematical model is attained. The major result of the presented model is that the rate of the entropy generation is boosted for the local inertial coefficient parameter. In a recent study, Adesanya et al.[58] performed the entropy generation appraisal for a couple stress fluid film flow on an inclined heated surface with viscous dissipation impacts. In this analysis, it is comprehended that the fluid temperature and velocity show opposing tendency versus the couple stress parameter. Furthermore, many investigators have worked on entropy generation analysis on a wide number of geometries that may found in[58–65].

The studies deliberated above reveal that abundant literature discussing the nanofluid flow of an extended cylinder is available under the influence of varied impacts. Nevertheless, comparatively less literature can be witnessed that discusses the flow of Maxwell nanofluid over an extended cylinder. But so far one has discussed the Maxwell nanofluid flow past an extended cylinder with thermal radiation, chemical reaction, and gyrotactic microorganisms with partial slip in a Darcy–Forchheimer spongy medium. The problem is solved numerically, and pertinent graphs are plotted versus the involved profiles with logical descriptions. Table 1 illustrates the originality/uniqueness of the stated fluid mathematical model by assessing it with the available researches.

Mathematical modeling

We examine an incompressible flow outside a cylinder having radius R and the constant temperature T_w. As the axial direction of a cylinder along the x-axis while radial direction along r-axis. A stretching surface of the cylinder has velocity $u_w = u_0(\frac{x}{l})$, where l is the characteristic length and u_0 shows the reference velocity. The flow situation induced by a magnetic field of intensity B_0 is displayed in Fig. 1.

The resulting boundary layer equations defining the depicted scenario are given as[66]:

$$\frac{\partial}{\partial x}(ru) + \frac{1}{r}\frac{\partial}{\partial r}(rv) = 0, \tag{1}$$

$$u\frac{\partial u}{\partial x} + v\frac{\partial u}{\partial r} = \nu\left(\frac{\partial^2 u}{\partial r^2} + \frac{1}{r}\frac{\partial u}{\partial r}\right) + \lambda^*\left[u^2\frac{\partial^2 u}{\partial x^2} + 2uv\frac{\partial^2 u}{\partial x \partial r} + v^2\frac{\partial^2 u}{\partial r^2}\right] - \frac{\sigma_1}{\rho}B_0^2 u - \frac{\nu}{k_2}u - Fu^2, \tag{2}$$

$$u\frac{\partial T}{\partial x}+v\frac{\partial T}{\partial r}=\frac{k}{\rho c_p}\left(\frac{1}{r}\frac{\partial T}{\partial r}+\frac{\partial^2 T}{\partial r^2}\right)+\tau\left[D_B\frac{\partial T}{\partial r}\frac{\partial C}{\partial r}+\frac{D_T}{T_\infty}\left(\frac{\partial T}{\partial r}\right)^2\right]-\frac{1}{\rho c_p}\frac{\partial q_r}{\partial r}, \tag{3}$$

$$u\frac{\partial C}{\partial x}+v\frac{\partial C}{\partial r}=D_B\left(\frac{\partial^2 C}{\partial r^2}+\frac{1}{r}\frac{\partial C}{\partial r}\right)+\frac{D_T}{T_\infty}\left(\frac{\partial^2 T}{\partial r^2}+\frac{1}{r}\frac{\partial T}{\partial r}\right)-\lambda_1(C-C_\infty)^n, \tag{4}$$

$$u\frac{\partial N}{\partial x}+v\frac{\partial N}{\partial r}=D_n\left(\frac{1}{r}\frac{\partial N}{\partial r}+\frac{\partial^2 N}{\partial r^2}\right)-\frac{\lambda w_c}{C_w-C_\infty}\left[\frac{\partial C}{\partial r}\frac{\partial N}{\partial r}+N\frac{\partial^2 C}{\partial r^2}\right]. \tag{5}$$

With boundary conditions[66]:

$$\begin{aligned}
&u=L_1 v\frac{\partial u}{\partial r}|_{r=R}+\ \mathrm{u}_w,\ \ v=0,\\
&T=L_2\frac{\partial T}{\partial r}|_{r=R}+T_w, C=L_3\frac{\partial C}{\partial r}+C_w.\\
&N=L_4\frac{\partial N}{\partial r}|_{r=R}+N_w\ \text{at}\ \ r=R,\\
&u=0,\ \mathrm{N}=N_\infty,\ \ C=C_\infty,\quad T=T_\infty,\ \text{as}\ \ \text{at}\ r=\infty,
\end{aligned} \tag{6}$$

The radiative heat flux q_r is given by:

$$q_r=\left(-\frac{4\sigma^*}{3k^*}\right)\frac{\partial T^4}{\partial r}=\left(-\frac{16\sigma^*}{3k^*}\right)T^3\frac{\partial T}{\partial r}. \tag{7}$$

The following transformation is used to obtain the non-dimensional structure of the above-mentioned flow model[66]:

$$\begin{aligned}
&\eta=\frac{r^2-R^2}{2R}\left(\frac{u_0}{lv}\right)^{\frac{1}{2}},\ \psi=\sqrt{\left(\frac{vu_0}{l}\right)}xRf(\eta),\ \theta(\eta)=\frac{T-T_\infty}{T_w-T_\infty},\\
&\xi(\eta)=\frac{N-N_\infty}{N_w-N_\infty},\ \phi(\eta)=\frac{C-C_\infty}{C_w-C_\infty},\ u=\frac{u_0}{l}xf^{'}(\eta),\ v=-\frac{1}{r}\sqrt{\frac{vu_0}{l}}Rf(\eta).
\end{aligned} \tag{8}$$

Equation (1) trivially fulfilled and Eqs. (2–6) are as follows:

$$\begin{aligned}
&(1+2M\eta)f'''+ff''-f'^2+2Mf''-\beta\left(f^2f''''-2ff''\right)\\
&-K^2f'-\lambda f'-Frf'^2=0,
\end{aligned} \tag{9}$$

$$\begin{aligned}
&\frac{1}{\mathrm{Pr}}\left[(1+2M\eta)\theta''+2M\theta'\right]+f\theta'+Nb(1+2M\eta)\theta'\phi'+Nt(1+2M\eta)\theta'^2\\
&+\frac{1}{\mathrm{Pr}}\frac{4}{3}Rd\left[\begin{aligned}&3(\theta_w-1)[1+(\theta_w-1)\theta]^2(1+2M\eta)\theta'^2+[1+(\theta_w-1)\theta]^3M\theta'\\&+[1+(\theta_w-1)\theta]^3(1+2M\eta)\theta''\end{aligned}\right]=0,
\end{aligned} \tag{10}$$

$$(1+2M\eta)\phi''+2M\phi'+Scf\phi'+\frac{Nt}{Nb}\left[(1+2M\eta)\theta''+2M\theta'\right]-Sc\gamma\phi^n=0, \tag{11}$$

$$\begin{aligned}
&(1+2M\eta)\xi^{''}+Lb\,\mathrm{Pr}f\xi^{'}+2M\xi^{'}\\
&-Pe\left(\begin{aligned}&\sigma M\phi^{'}+M\xi\phi^{'}+(1+2M\eta)\xi^{'}\phi^{'}\\&+\sigma(1+2M\eta)\phi^{''}+(1+2M\eta)\xi\phi^{''}\end{aligned}\right)=0.
\end{aligned} \tag{12}$$

$$\begin{aligned}
&f(0)=0, f^{'}(0)=B_1f^{''}(0)+1,\ \theta(0)=B_2\theta^{'}(0)+1,\\
&\phi(0)=B_3\phi^{'}(0)+1,\ \xi(0)=B_4(0)\xi'(0)+1,\\
&f^{'}=0,\ \theta=0,\ \phi=0,\ \xi=0.
\end{aligned} \tag{13}$$

Particular dimensionless parameters emerging in the above equations are portrayed as:

$$
\begin{aligned}
&M=\left(\frac{l\nu}{u_0R^2}\right)^{\frac{1}{2}},\quad K=\left(\frac{\sigma_1B_0^2l}{\rho u_0}\right)^{\frac{1}{2}},\quad B_1=L_1\left(\frac{u_0\nu}{l}\right)^{\frac{1}{2}},\quad B_2=L_2\left(\frac{u_0}{l\nu}\right)^{\frac{1}{2}},\quad B_3=L_3\left(\frac{u_0}{l\nu}\right)^{\frac{1}{2}},\\
&\theta_w=\frac{T_w}{T_\infty},\quad \gamma=\frac{\lambda_1 l}{u_0},\quad Nb=\frac{\tau D_B(C_w-C_\infty)}{\nu},\quad Nt=\frac{\tau D_T(T_w-T_\infty)}{\nu T_\infty},\quad \beta=\frac{\lambda^* u_0}{l},\\
&\lambda=\frac{\nu l}{k_2u_0},\quad Fr=\frac{c_b}{\sqrt{k_2}},\quad Rd=\left(\frac{4\sigma^*T_\infty^3}{kk^*}\right),\quad Sc=\frac{\nu}{D_B},\quad Pe=\frac{\lambda w_c}{D_n},\\
&Lb=\frac{\alpha}{D_n},\quad \mathrm{Pr}=\frac{\nu}{\alpha},\quad \sigma=\frac{N_\infty}{N_w-N_\infty},
\end{aligned}
\tag{14}
$$

The dimensional form of drag force coefficients, rate of mass transfer, rate of heat transfer, and Motile microorganisms are appended as below:

$$
C_{f_x}=\frac{\mu\left(\frac{\partial u}{\partial r}+\frac{\partial v}{\partial x}\right)_{r=R}}{\rho u_w^2},\ \mathrm{Sh}_x=\frac{xj_w}{D_m(C_w-C_\infty)},\ \mathrm{Nu}_x=\frac{xq_w}{k(T_w-T_\infty)},\ \mathrm{Nn}_x=\frac{xq_n}{D_n\Delta N}.
\tag{15}
$$

With

$$
q_w=-k\left(\frac{\partial T}{\partial r}\right)_{r=R}+(q_r)_w,\ j_w=-D_m\left(\frac{\partial C}{\partial r}\right)_{r=R},\ q_n=-D_n\left(\frac{\partial N}{\partial r}\right)_{r=a},
\tag{16}
$$

The Drag force coefficient, mass transfer rate, Motile microorganism, and rate of heat in the dimensionless form are supplemented below:

$$
\begin{aligned}
&\mathrm{Re}_x^{\frac{1}{2}}C_{f_x}=f''(0),\ \mathrm{Re}_x^{-\frac{1}{2}}Sh_x=-\phi'(0),\\
&\mathrm{Re}_x^{-\frac{1}{2}}Nu_x=-\left(1+\frac{4}{3}Rd(1+(\theta_w-1)\theta(0))\right)^3,\theta'(0),\ \mathrm{Nn}_x=-\xi'(0),
\end{aligned}
\tag{17}
$$

Rate of entropy generation (EG)

The volumetric equation is represented as:

$$
\begin{aligned}
S_G=&\frac{k}{T_\infty^2}\left(\frac{\partial T}{\partial r}+\left(\frac{16\sigma T^3}{3k^*}\right)\left(\frac{\partial T}{\partial r}\right)^2\right)+\frac{\mu}{T_\infty}\left(\frac{\partial u}{\partial r}\right)^2+\frac{\sigma B_0^2u^2}{T_\infty\rho}+\frac{Rd}{C_\infty}\left(\frac{\partial C}{\partial r}\right)^2+\frac{Rd}{T_\infty}\left(\frac{\partial T}{\partial r}\right)\left(\frac{\partial C}{\partial r}\right)\\
&+\frac{Rd}{N_\infty}\left(\frac{\partial N}{\partial r}\right)^2+\frac{Rd}{C_\infty}\left(\frac{\partial N}{\partial r}\right)\left(\frac{\partial C}{\partial r}\right).
\end{aligned}
\tag{18}
$$

The characteristics EG is framed as:

$$
S'''=\frac{\nabla T^2k}{T_\infty^2l^2}
\tag{19}
$$

The entropy generation N_G is given as the quotient of the S_G and S''', i.e.,

$$
N_G=\left(\frac{S_G}{S'''}\right)
\tag{20}
$$

In dimensionless form:

$$
\begin{aligned}
N_G=\left(\frac{S_G}{S'''}\right)=&(1+2M\eta)\alpha_1\mathrm{Re}\theta'^2+(1+2M\eta)Br\mathrm{Re}f''^2+MBr\mathrm{Re}f'^2\\
&+(1+2M\eta)L\mathrm{Re}\theta'\phi'+(1+2M\eta)L_5\mathrm{Re}\frac{\alpha_3}{\alpha_1}\xi'^2+(1+2M\eta)L_5\mathrm{Re}\frac{\alpha_2}{\alpha_1}\xi'\phi'.
\end{aligned}
\tag{21}
$$

The parameters used in Eq. (22) are defined as:

$$
\begin{aligned}
&\alpha_1=\frac{T_w-T_\infty}{T_\infty},\quad \alpha_2=\frac{C_w-C_\infty}{C_\infty},\quad \alpha_3=\frac{N_w-N_\infty}{N_\infty},\quad L=\left(\frac{Rd(C_w-C_\infty)}{k}\right)\\
&L_5=\left(\frac{Rd(N_w-N_\infty)}{k}\right),\quad Br=\left(\frac{\mu_0a^2x^2}{k\Delta T}\right),\quad N_G=\left(\frac{S_GT_\infty\nu}{k\Delta Ta}\right),\quad \mathrm{Re}=\frac{U_0l^2}{\nu}.
\end{aligned}
\tag{22}
$$

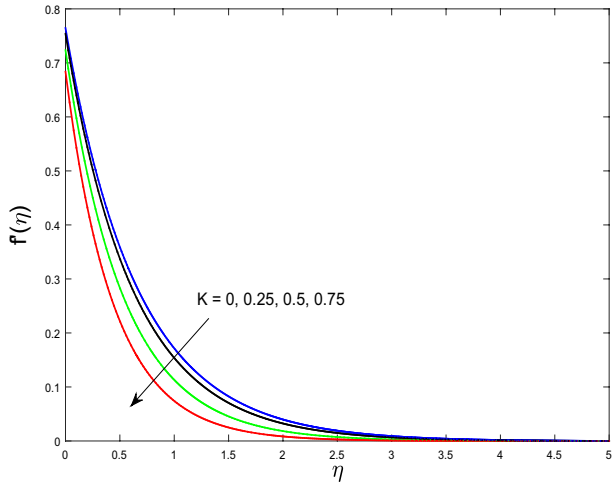

Figure 2. Plot of $f^{'}$ for K.

Numerical procedure

For the nonlinear arrangement of equations and boundary conditions (9)–(13) the finite difference MATLAB bvp4c procedure is applied which is solid at 4th order and the grid size of 0.01 is viewed as acknowledged 10^{-6}. The numerical plan requires the change of higher-order differential equations into one-order differential equations.

$$\begin{aligned} &y_1 = f, y_2 = f', y_3 = f'', yy_1 = f''', y_4 = \theta, y_5 = \theta', yy_2 = \theta'', \\ &y_6 = \phi, y_7 = \phi', yy_3 = \phi'', y_8 = \xi, y_9 = \xi', yy_4 = \xi'', \end{aligned} \tag{23}$$

$$\begin{aligned} yy_1 = \Bigg(&\frac{\left(-y_1y_3 + y_2^2 - 2My_3 + \beta\left(y_1y_3 - 2y_1y_3\right)\right) + K^2y_2 + \lambda y_1 + Fry_2y_2}{1 + 2M\eta} - \Bigg); \\ &\left(-2\gamma y_5 - \Pr y_1y_5 - \Pr\left(1 + 2M\eta\right)\left(N_by_5y_7 + N_ty_5^2\right)\right) \end{aligned} \tag{24}$$

$$yy_2 = \frac{-\frac{4}{3}Rd\left[3[\theta_w - 1]\left(1 + [\theta_w - 1]y_4\right)^2(1 + 2M\eta)y_5^2 + \left(1 + y_4[\theta_w - 1]\right)^3My_5\right]}{(1 + 2M\eta) + \frac{4}{3}Rd\left(1 + [\theta_w - 1]y_4\right)^3(1 + 2M\eta)}; \tag{25}$$

$$yy_3 = \left(\frac{-2My_7 - Scy_1y_7 - \frac{N_t}{N_b}\left(2My_5 + (1 + 2M\eta yy_2\right) + ScMy_6^{\eta}}{(1 + 2\gamma\eta)}\right); \tag{26}$$

$$yy_4 = \frac{\left(-2My_9 - Lb\Pr y_1y_9\right) + Pe\begin{pmatrix}(1 + 2M\eta)y_9y_6 + My_8y_7 + \sigma My_7 \\ \sigma(1 + 2M\eta)y_8yy_3 + (1 + 2M\eta)y_8yy_3\end{pmatrix}}{(1 + 2M\eta)}; \tag{27}$$

$$\begin{aligned} &y_2(0) - 1; y_2(0) - 1 - B_1y_3(0); y_4(0) - 1 - B_2y_5(0); y_6(0) - 1 - B_3y_7(0); \\ &y_8(0) - 1 - B_4y_9(0); y_2(\infty); y_4(\infty); y_6(\infty); y_8(\infty); \end{aligned} \tag{28}$$

Results with discussion

In this segment, we will examine the effect of distinct parameters on velocity, concentration, temperature, and gyrotactic microorganism fields. The numerous parameters like the magnetic interaction parameter (K), Darcy parameter (Fr), radiation parameter (Rd), Schmidt number (Sc), temperature ratio parameter (θ_w), porosity parameter (λ), Deborah number (β), thermophoresis parameter (Nt), curvature parameter (M), bioconvection Lewis number (Lb), Prandtl number (Pr), Brownian motion parameter (Nb), wall roughness parameter (B_1), chemical reaction parameter (γ), concentration slip parameter (B_3), thermal slip parameter (B_3), Peclet number (Pe), Bioconvection parameter (σ), and reaction order n are discussed on temperature, velocity and nanoparticles concentration, and gyrotactic microorganism fields. Figure 2 demonstrated the behavior of K on the $f^{'}(\eta)$. The strength of the Lorentz force is measured by K. The increase in K enhances the Lorentz force strength and due to the rise in K the velocity in axial direction decreases. As a result, the gradient of velocity at the surface

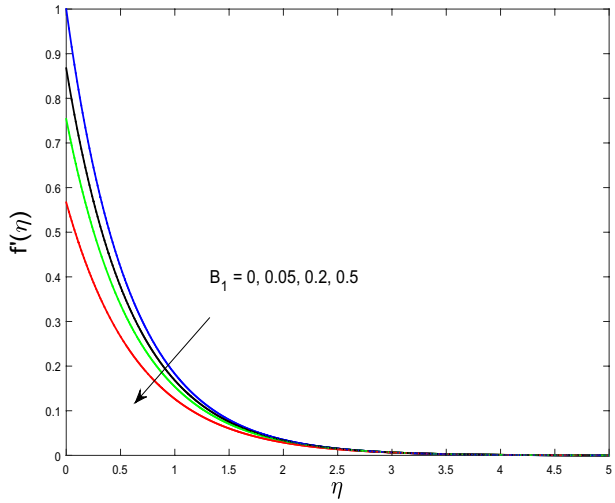

Figure 3. Plot of $f^{'}$ for B_1.

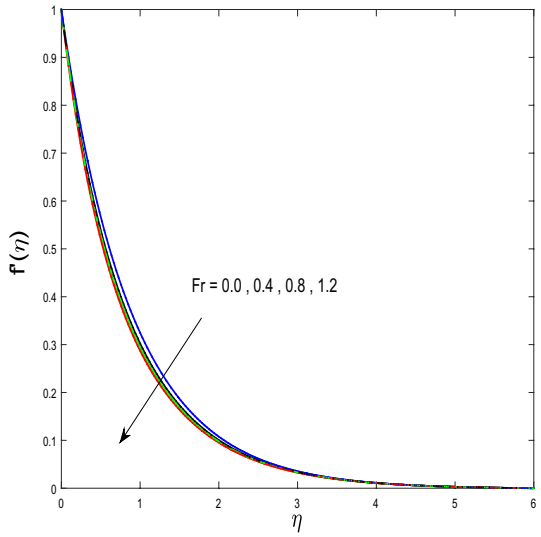

Figure 4. Plot of $f^{'}$ for Fr.

is decreased. The wall B_1 effect on the velocity profile is described in Fig. 3. The slip decreases the speed close to the disk and this condition enhances by increasing in K. Practically, the stretched impact of a cylinder is moderately shifted to the liquid layers which result in a decrease in $f^{'}(\eta)$. The influence of Fr on the velocity field $f^{'}(\eta)$ is investigated in Fig. 4. It is examined that by escalating the variations of Fr, the decreasing trend of the velocity field is seen. This is because the higher values of Fr produce resistance in a liquid flow and hence velocity decreases. Figure 5 demonstrated the effect of the λ on the velocity distribution of $f^{'}(\eta)$. The liquid's velocity diminishes on greater estimations of the λ. Actually, the movement of the liquid is stalled because of the presence of permeable media, and this results in the falloff of the liquid velocity. The effect of β on the velocity field $f^{'}(\eta)$ is investigated in Fig. 6. It is examined that by escalating the variations of β, the diminishing behavior of the velocity field is seen. The impact of the θ_w upon $\theta(\eta)$ is explained by Fig. 7. A significant increase in $\theta(\eta)$ is observed. Enhancing θ_w signifies the temperature of the wall that causes thicker penetration depth for temperature profile. Likewise, the thermal diffusivity lies in the boundary layer with the relating exchange of heat. The thermal boundary layer corresponds to be larger nearby the region where the hotness is larger while it is lower a long way from cylinder because here temperature is low when compared to others. Subsequently, an intonation point emerges on the region when greater θ_w is considered. The temperature field for numerous M is shown in Fig. 8. A generous upgrade in the temperature of the liquid is seen when the radius of the cylinder is reduced. The effect of Pr on the thermal profile is described in Fig. 9. It is observed that the existence of melting phenomenon of the liquid temperature increases with rising variations of Pr. Therefore, we can judge that greater variation of Pr enhances the temperature field. Figure 10 defines that the large estimation of the B_2 descends the dimensionless liquid's temperature. From the figure, it is noticed that the thermal boundary layer becomes thicker

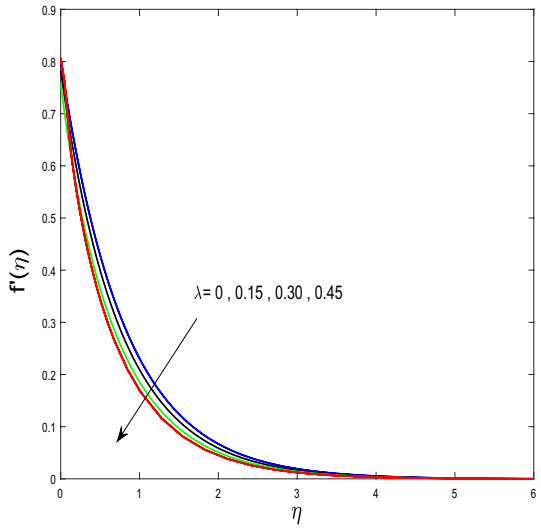

Figure 5. Plot of $f^{'}$ for λ.

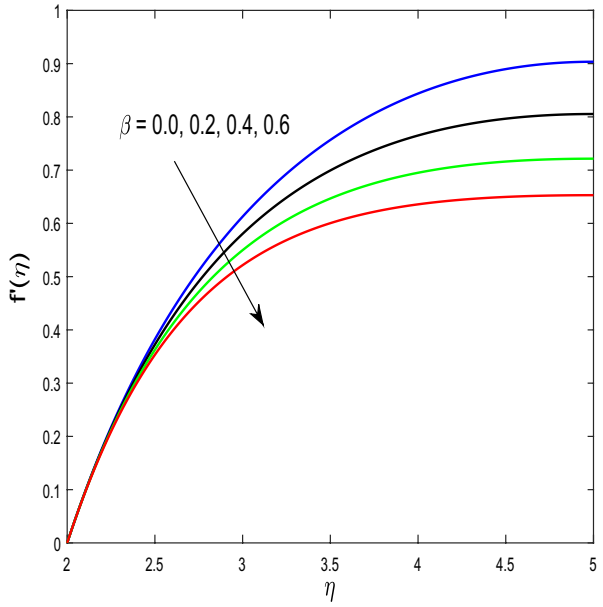

Figure 6. Plot of $f^{'}$ for β.

on enhancing the values of the curvature parameter. Figure 11 is outlined to show the plots of $\theta(\eta)$ for numerous terms of *Rd* when other variables are fixed. It can be judged that growing values of *Rd* increase the temperature and its parallel thickness of layer become thicker. Figure 12 elucidates that an increment in *Sc* decays the nanoparticle concentration distribution $\phi(\eta)$. There is an opposite relationship between the *Sc* and the Brownian diffusion coefficient. Greater the values of Schmidt number *Sc* lower will be the Brownian diffusion coefficient, which tends to decrease the $\phi(\eta)$. Figure 13 portrays the concentration field for different estimations of γ. Large variations of the γ tend to smaller the nanoparticle concentration field. The descending behavior of a concentration profile $\phi(\eta)$ on a B_3 is drawn in Fig. 14. Figure 15 demonstrated that for greater values of reaction order *n* the concentration profile becomes higher. Figure 16 depicts the influence of *Nt* on $\phi(\eta)$. Both the concentration and thermal layer thickness are increased by accumulating the variations of the *Nt*. Greater estimations of the *Nt* give rise to thermophoresis force which increases the movement of nanoparticles from cold to hot surfaces and also increases in the thermal layer thickness. The descending behavior in concentration distribution $\phi(\eta)$ against *Nb* is shown in Fig. 17. An enhancement in *Nb* increases the Brownian motion due to which there is an escalation in the movement of nanoparticles and hence boundary layer thickness reduces. Figure 18 plotted to draw the curves of $\xi(\eta)$ for different terms of *Lb* while other variables are fixed. It is observed that *Lb* depicts the decreasing behavior for large values of *Lb*. Figure 19 shows the behavior of *Pe* on gyrotactic microorganisms'

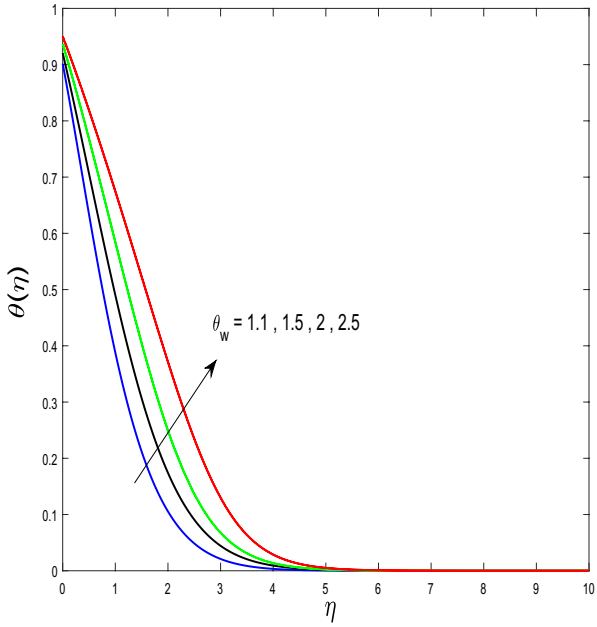

Figure 7. Plot of θ for θ_w.

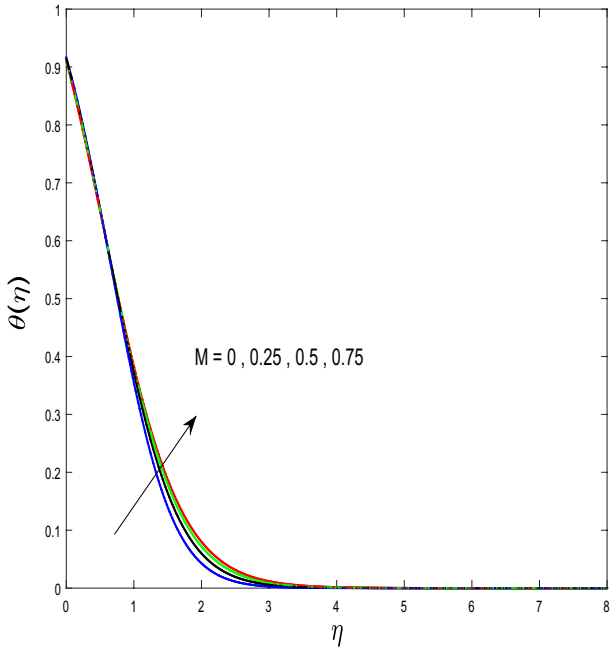

Figure 8. Plot of θ for M.

profile $\xi(\eta)$. Here, $\xi(\eta)$ is an increasing function of Pe that effects to a decrease the diffusivity of microorganisms. Figure 20 indicates the variations in gyrotactic microorganism profile $\xi(\eta)$ for distinct estimations of theσ. Large variations of σ decrease the gyrotactic microorganism field. Figure 21 is drawn to illustrates the impact of the Brinkman numbers on the Entropy generation number. It is found that Entropy escalates for the Brinkman number. In Fig. 22, with rising estimations of Re, an increase is seen in the entropy generation number. A higher Re causes more aggravation in the field and expand fluid friction and heat transfer, which eventually increases the rate of entropy in the boundary layer region.

Table 2 is generated to substantiate the outlined results in this study by comparing it with Khan and Mustafa[68] and Tamoor et al.[56] in limiting case. A good agreement between the two outcomes is seen. Besides, Tables 3, 4, 5 express the numerical variations of the local Sherwood number Sh_x, local Nusselt number Nu_x, and density amount of motile microorganism Nn_x for distinct estimations of K, M, θ_w, Rd, Pr, B_1, B_2, Sc, γ, k, Pe, Lb, and σ.

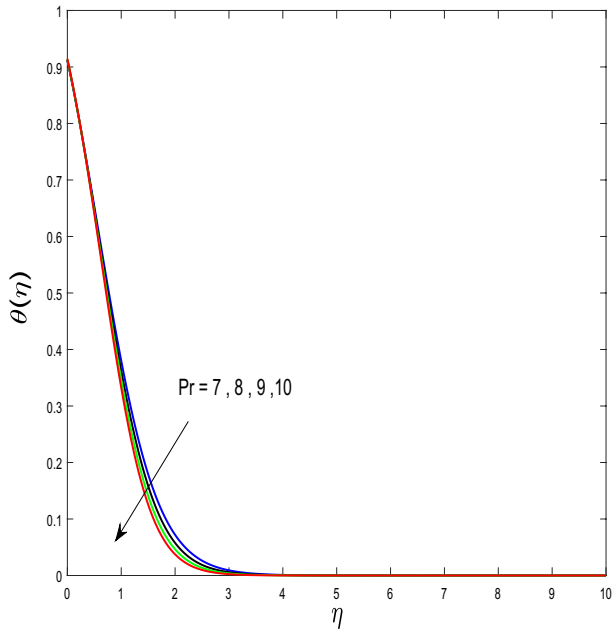

Figure 9. Plot of θ for Pr.

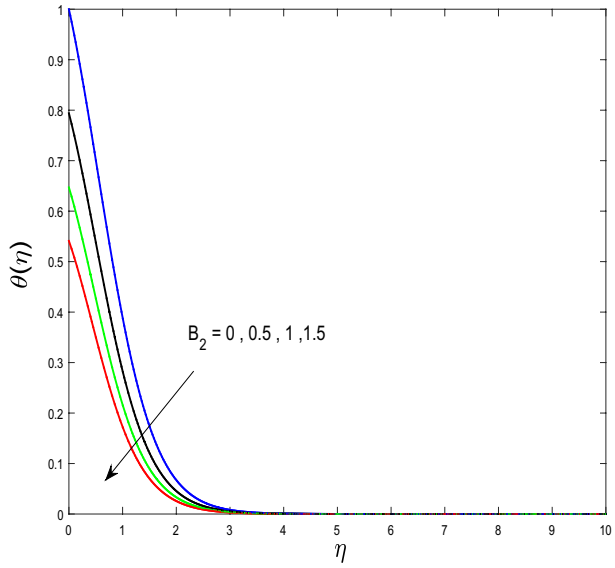

Figure 10. Plot of θ for B_2.

It is witnessed in Table 3 here that the heat flux rate is escalated for the growing estimates of K, but the opposite trend is perceived for the estimations of M, θ_w, Rd. In Table 4, it is witnessed that the mass flux rate is declined for the values of the Sc, and γ, however, it is enhanced for the increasing estimates of the M and n. The behavior of the varied parameters versus the density amount of motile microorganism is portrayed in Table 5. It is renowned that density amount of motile microorganism is improved for the estimations of M, Pr, σ, Pe, and Lb.

Concluding remarks

In the current investigation, we have discussed nonlinear radiative MHD Williamson nano liquid flow via a stretched cylinder in a Darcy–Forchheimer porous media. The flow is assisted by the impacts of the chemical reaction, and gyrotactic microorganisms with partial slip condition at the boundary. The solution to the problem

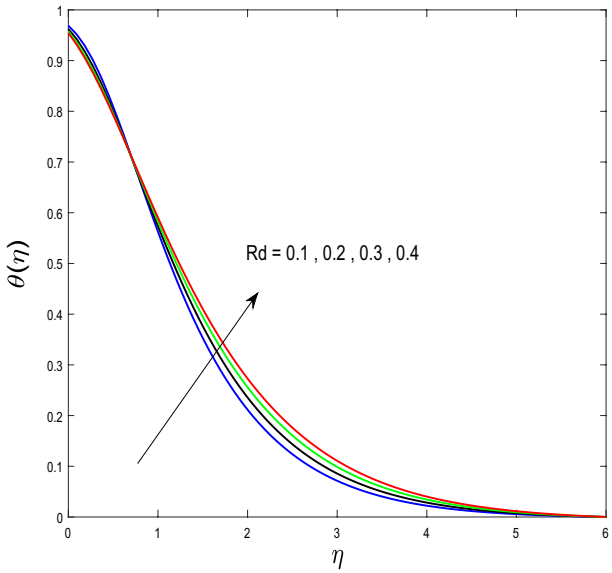

Figure 11. Plot of θ for Rd.

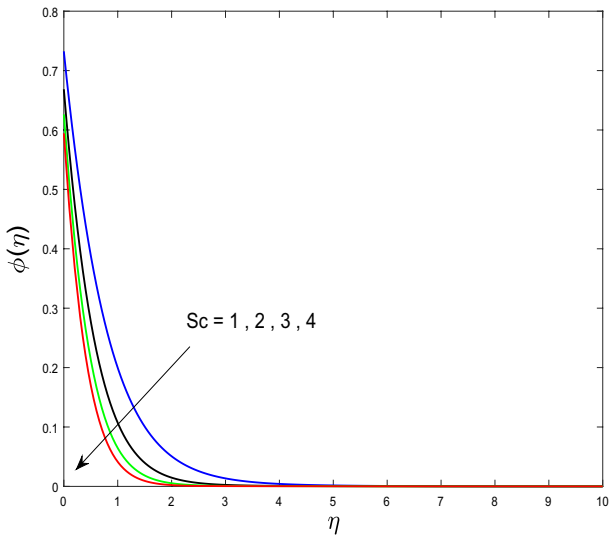

Figure 12. Plot of ϕ for Sc.

is addressed by the MATLAB scheme of the bvp4c built-in function. The main results of the present investigation are appended below:

- Nb and Nt show the opposing nature against the concentration field.
- The velocity distribution is lowered for large variations of K, Fr, and λ.
- Pe decreases the gyrotactic microorganism profile.
- An increment in Sc,B_3, and γ leads to a lowering concentration profile.
- Enhanced variations of Pr and B_2 display the decreasing behavior on the temperature profile.
- Large values of θ_w, Rd, and M causes an increment in temperature distribution.
- Gyrotactic microorganism profile reduces for greater variations of Lb and σ.
- Entropy intensifies for Br; however, an opposite tendency is observed for β.

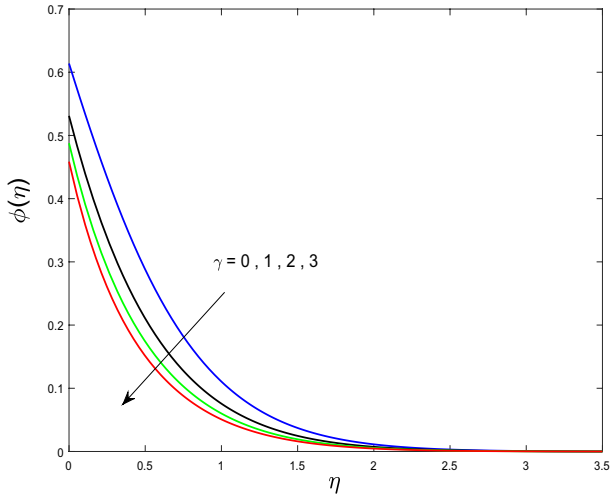

Figure 13. Plot of ϕ for γ.

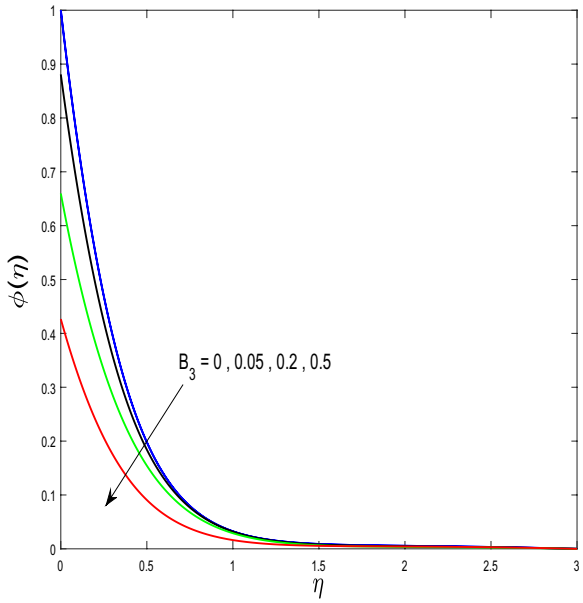

Figure 14. Behaviour of ϕ for B_3.

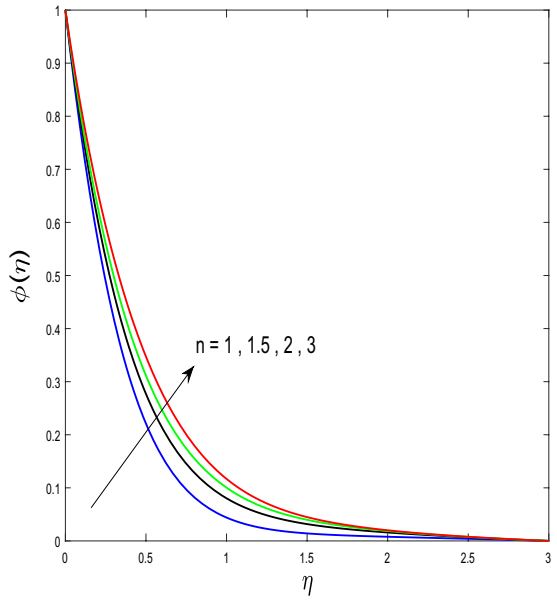

Figure 15. Plot of ϕ for n.

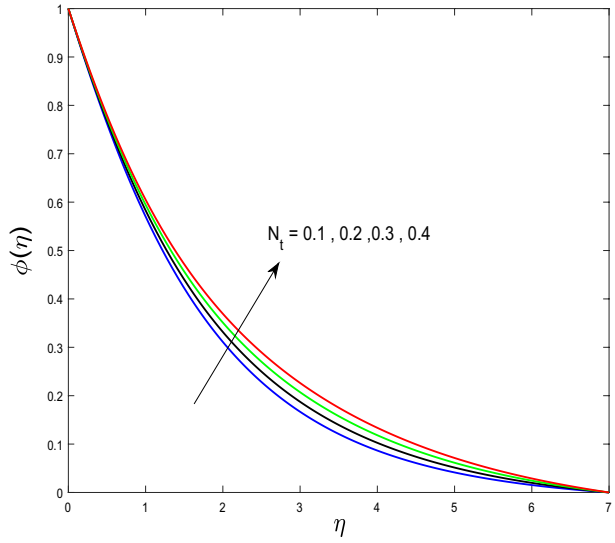

Figure 16. Plot of ϕ for Nt.

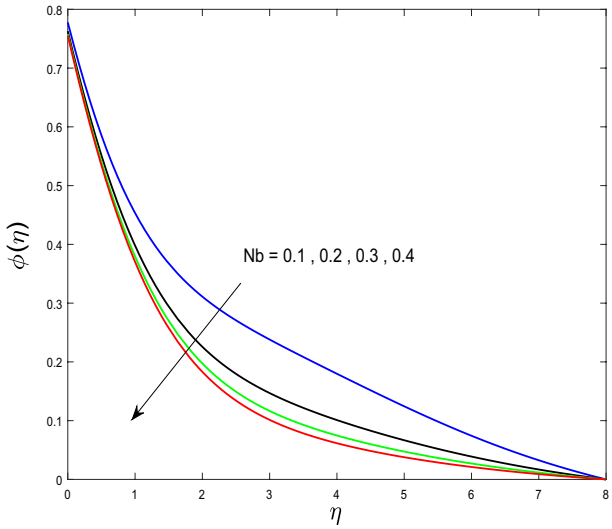

Figure 17. Plot of ϕ for *Nb*.

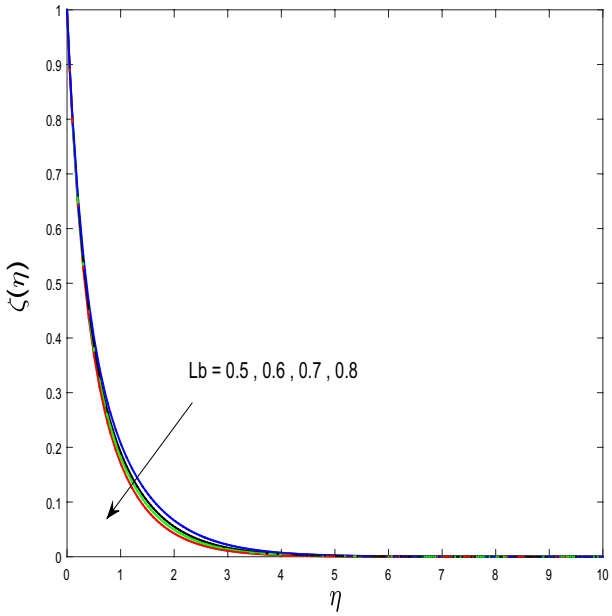

Figure 18. Plot of ξ for *Lb*.

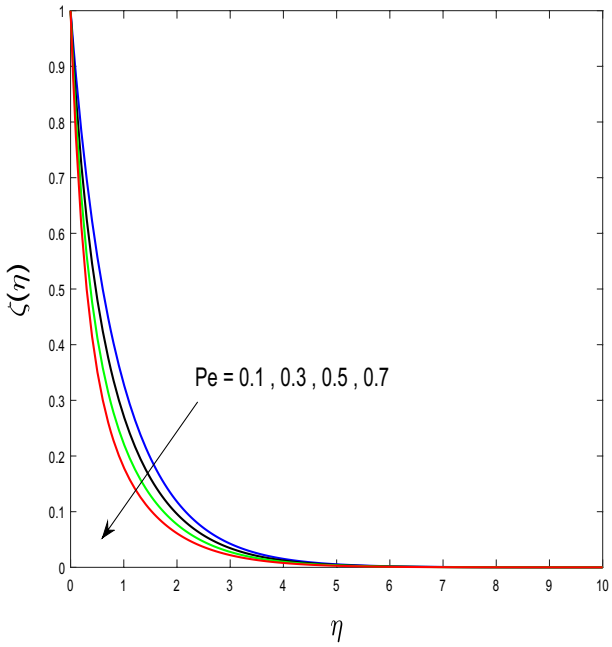

Figure 19. Plot of ξ for *Pe*.

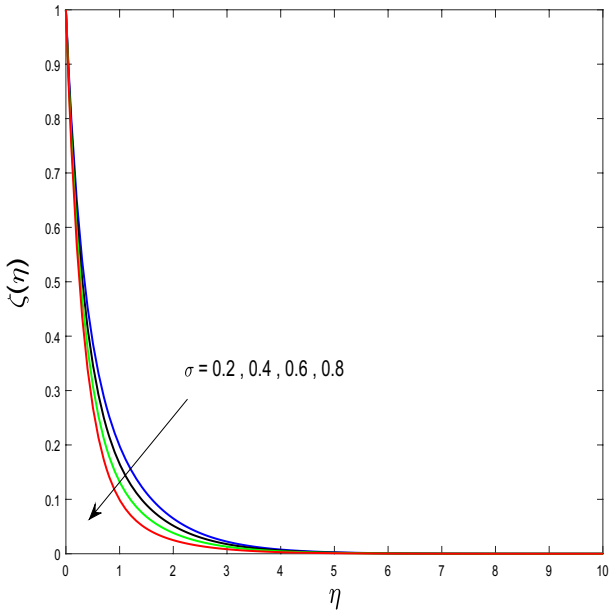

Figure 20. Plot of ξ for σ.

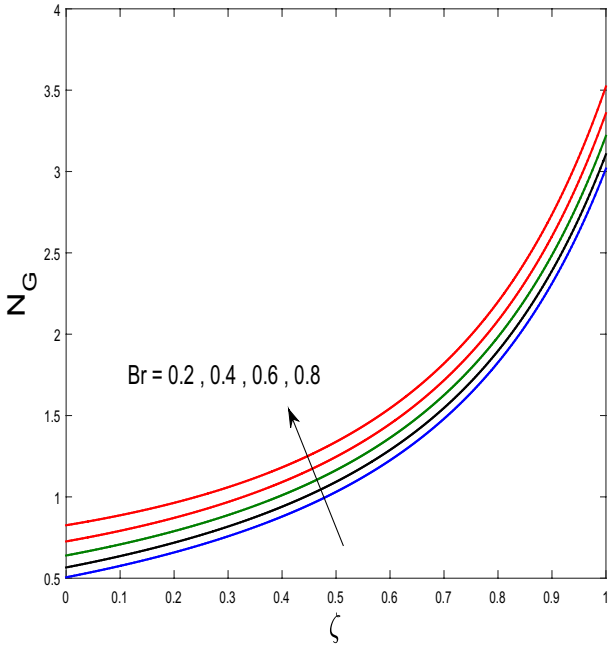

Figure 21. Plot of N_G for Br.

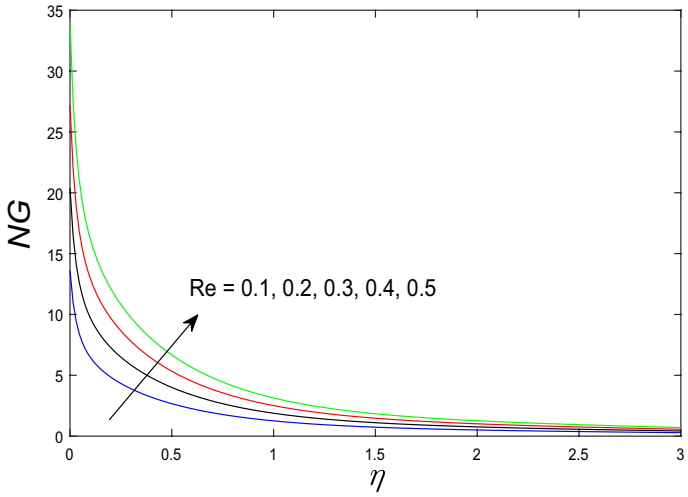

Figure 22. Plot of N_G for Re.

K	$-f''(0)$ [68]	$-f''(0)$ [56]	$-f''(0)$ Present
0	1	1	1
0.2	1.0198039	1.01980	1.01981
0.5	1.1180340	1.11803	1.11803
0.8	1.2806248	1.28063	1.28062
1	1.4142136	1.41421	1.41421

Table 2. Validation of numerical outcomes for $-f''(0)$ with Khan and Mustafa[68] and Tamoor et al.[56] and when $M = B_1 = 0$.

K	M	θ_w	Rd	$(\mathrm{Re}_x)^{-\frac{1}{2}} Nu_x$
0.5	0.2	1.5		0.7654
1				0.6803
1.5				0.5851
2				0.5003
	0.5			0.7745
	0.7			0.7801
	1			0.7883
		2		1.1440
		2.5		1.4871
		3		1.7770
			0.1	1.3736
			0.3	2.2339
			0.5	3.3713

Table 3. Computations of $(\mathrm{Re}_x)^{\frac{1}{2}} Nu_x$ for various variations of K, M, θ_w, Rd when $\mathrm{Pr} = 7$ and $B_1 = B_2 = 0.5$.

M	Sc	γ	n	$(\mathrm{Re}_x)^{-\frac{1}{2}} Sh_x$
0.2	5	1	1	1.15817
0.5				1.17480
0.7				1.18683
1				1.20568
	2			0.97565
	3			1.05478
	7			1.22726
		2		1.27036
		3		1.34142
		4		1.39264
			2	0.99641
			3	0.92496
			5	0.87854

Table 4. Computations of $(\mathrm{Re}_x)^{-\frac{1}{2}} Sh_x$ for numerous variations of Sc,M, and γ when $\mathrm{Pr} = 7$, $k = 0.5$ and $B_1 = B_2 = B_3 = 0.5$.

M	Pr	σ	Pe	Lb	$(\mathrm{Re}_x)^{-\frac{1}{2}} Nn_x$
0.3	1.5	0.2	0.3	0.2	0.935596
0.6					1.059580
0.9					1.193600
	1.0				0.915801
	1.5				0.935596
	2.0				0.940771
		0.2			0.935596
		0.4			1.012580
		0.6			1.089560
			0.4		1.065290
			0.5		1.189010
			0.6		1.307130
				0.3	0.963155
				0.6	1.038210
				0.9	1.103780

Table 5. Computations of $(\mathrm{Re}_x)^{-\frac{1}{2}} Nn_x$ for various variations of M, Pr, σ, Pe and Lb.

Received: 21 January 2021; Accepted: 19 April 2021
Published online: 30 April 2021

References

1. Choi, S. U. S., & Eastman, J. A. Enhancing thermal conductivity of fluids with nanoparticles. *(IMECE). 66*, 99–105 (1995).
2. Koo, J. & Kleinstreuer, C. Laminar nanofluid flow in microheat-sinks. *Int. J. Heat Mass Transf.* **48**(13), 2652–2661 (2005).
3. Eastman, J. A., Choi, S. U. S., Li, S., Yu, W. & Thompson, L. J. Anomalously increased effective thermal conductivities of ethylene glycol-based nanofluids containing copper nanoparticles. *Appl. Phys. Lett.* **78**(6), 718–720 (2001).
4. Choi, S. U. S., Zhang, Z. G., Yu, W., Lockwood, F. E. & Grulke, E. A. Anomalous thermal conductivity enhancement in nanotube suspensions. *Appl. Phys. Lett.* **79**(14), 2252–2254 (2001).
5. Bilal, M., Mazhar, S. Z., Ramzan, M. & Mehmood, Y. Time-dependent hydromagnetic stagnation point flow of a Maxwell nanofluid with melting heat effect and amended Fourier and Fick's laws. *Heat Trans.* https://doi.org/10.1002/htj.22081 (2021).
6. Tlili, I., Naseer, S., Ramzan, M., Kadry, S. & Nam, Y. Effects of chemical species and nonlinear thermal radiation with 3D Maxwell nanofluid flow with double stratification—an analytical solution. *Entropy* **22**(4), 453 (2020).
7. Sheikholeslami, M., Arabkoohsar, A., & Jafaryar, M. (2020). Impact of a helical-twisting device on the thermal--hydraulic performance of a nanofluid flow through a tube. *J. Therm. Anal. Calorim.* **139**(5), 3317–3329 (2020).
8. Farooq, U. *et al.* MHD flow of Maxwell fluid with nanomaterials due to an exponentially stretching surface. *Sci. Rep.* **9**(1), 1–11 (2019).
9. Ramesh, G. K., Shehzad, S. A., Rauf, A. & Chamkha, A. J. Heat transport analysis of aluminum alloy and magnetite graphene oxide through permeable cylinder with heat source/sink. *Phys. Scr.* **95**(9), 095203 (2020).
10. Reza-E-Rabbi, S., Ahmmed, S. F., Arifuzzaman, S. M., Sarkar, T. & Khan, M. S. Computational modelling of multiphase fluid flow behaviour over a stretching sheet in the presence of nanoparticles. *Int. J. Eng. Sci. Technol.* **23**(3), 605–617 (2020).
11. Abbasi, A., Mabood, F., Farooq, W. & Hussain, Z. Non-orthogonal stagnation point flow of Maxwell nano-material over a stretching cylinder. *Int. Comm. Heat Mass. Tran.* **120**, 105043 (2021).
12. Li, F. *et al.* Numerical study for nanofluid behavior inside a storage finned enclosure involving melting process. *J. Mol. Liq.* **297**, 111939 (2020).
13. Komeilibirjandi, A., Raffiee, A. H., Maleki, A., Nazari, M. A. & Shadloo, M. S. Thermal conductivity prediction of nanofluids containing CuO nanoparticles by using correlation and artificial neural network. *J. Therm. Anal. Calorim.* **139**(4), 2679–2689 (2020).
14. Waqas, H., Imran, M. & Bhatti, M. M. Influence of bioconvection on Maxwell nanofluid flow with the swimming of motile microorganisms over a vertical rotating cylinder. *Chin. J. Phys.* **68**, 558–577 (2020).
15. Islam, S., Khan, A., Kumam, P., Alrabaiah, H., Shah, Z., Khan, W., & Jawad, M. Radiative mixed convection flow of Maxwell nanofluid over a stretching cylinder with Joule heating and heat source/sink effects. *Sci. Rep. 10*(1), 1–18 (2020).
16. Ahmed, A., Khan, M. & Ahmed, J. Thermal analysis in swirl motion of Maxwell nanofluid over a rotating circular cylinder. *Appl. Math. Mech.* **41**(9), 1417–1430 (2020).
17. Kumar, R. V., Gowda, R. P., Kumar, R. N., Radhika, M. & Prasannakumara, B. C. Two-phase flow of dusty fluid with suspended hybrid nanoparticles over a stretching cylinder with modified Fourier heat flux. *Appl. Sci.* **3**(3), 1–9 (2021).
18. Kumar, R. N., Gowda, R. P., Abusorrah, A. M., Mahrous, Y. M., Abu-Hamdeh, N. H., Issakhov, A., & Prasannakumara, B. C. Impact of magnetic dipole on ferromagnetic hybrid nanofluid flow over a stretching cylinder. *Phys. Scr*. **96**(4), 045215 (2021).
19. Jayadevamurthy, P. G. R., Rangaswamy, N. K., Prasannakumara, B. C., & Nisar, K. S. Emphasis on unsteady dynamics of bioconvective hybrid nanofluid flow over an upward–downward moving rotating disk. *Num. Methods Part. Diff. Equ.* (2020).
20. Khan, S. U., Shehzad, S. A., & Ali, N. Bioconvection flow of magnetized Williamson nanoliquid with motile organisms and variable thermal conductivity. *Appl. Nanosci*. 1–12 (2020).
21. Ramesh, G. K., Gireesha, B. J. & Gorla, R. S. R. Study on Sakiadis and Blasius flows of Williamson fluid with convective boundary condition. *Nonlinear Eng.* **4**(4), 215–221 (2015).
22. Anwar, M. I., Rafique, K., Misiran, M., Shehzad, S. A., & Ramesh, G. K. Keller-box analysis of inclination flow of magnetized Williamson nanofluid. *Appl. Sci*. **2**(3), 1–9 (2020).
23. Darcy, H. Les fontaines publiques de la ville de Dijon: exposition et application...Victor Dalmont (1856).
24. Forchheimer, P. Wasserbewegung durch boden. Z. Ver. Deutsch, Ing., 45, 1782–1788 (1901).
25. Muskat, M. The flow of homogeneous fluids through porous media (No. 532.5 M88) (1946).
26. Pal, D. & Mondal, H. Hydromagnetic convective diffusion of species in Darcy–Forchheimer porous medium with non-uniform heat source/sink and variable viscosity. *Int. Commun. Heat Mass Transf.* **39**(7), 913–917 (2012).
27. Ganesh, N. V., Hakeem, A. A. & Ganga, B. Darcy–Forchheimer flow of hydromagneticnanofluid over a stretching/shrinking sheet in a thermally stratified porous medium with second order slip, viscous and Ohmic dissipations effects. *Ain Shams Eng. J.* **9**(4), 939–951 (2016).
28. Alshomrani, A. S. & Ullah, M. Z. Effects of homogeneous-heterogeneous reactions and convective condition in Darcy–Forchheimer flow of carbon nanotubes. *J. Heat Transfer.* **141**(1), 012405 (2019).
29. Saif, R. S., Hayat, T., Ellahi, R., Muhammad, T., & Alsaedi, A. Darcy–Forchheimerflow of nanofluid due to a curved stretching surface. *Int. J. Num. Method H*. **29**, (2018).
30. Seth, G. S., Kumar, R. & Bhattacharyya, A. Entropy generation of dissipative flow of carbon nanotubes in rotating frame with Darcy–Forchheimer porous medium: A numerical study. *J. Mol. Liq.* **268**, 637–646 (2018).
31. Hayat, T., Ra…que, K., Muhammad, T., Alsaedi, A., & Ayub, M. Carbon nanotubessignificance in Darcy–Forchheimer flow. *Res. Phys*. **8**, 26–33 (2018).
32. Ramesh, G. K., Kumar, K. G., Gireesha, B. J., Shehzad, S. A. & Abbasi, F. M. Magnetohydrodynamic nanoliquid due to unsteady contracting cylinder with uniform heat generation/absorption and convective condition. *Alex. Eng. J.* **57**(4), 3333–3340 (2018).
33. Arifuzzaman, S. M. *et al.* Hydrodynamic stability and heat and mass transfer flow analysis of MHD radiative fourth-grade fluid through porous plate with chemical reaction. *King Saud Univ. Sci.* **31**(4), 1388–1398 (2019).
34. Reza-E-Rabbi, S., Arifuzzaman, S. M., Sarkar, T., Khan, M. S. & Ahmmed, S. F. Explicit finite difference analysis of an unsteady MHD flow of a chemically reacting Casson fluid past a stretching sheet with Brownian motion and thermophoresis effects. *J. King Saud Univ. Sci.* **32**(1), 690–701 (2020).
35. Arifuzzaman, S. M., Khan, M. S., Mehedi, M. F. U., Rana, B. M. J. & Ahmmed, S. F. Chemically reactive and naturally convective high speed MHD fluid flow through an oscillatory vertical porous plate with heat and radiation absorption effect. *Eng. Sci. Technol.* **21**(2), 215–228 (2018).
36. Shankaralingappa, B. M., Gireesha, B. J., Prasannakumara, B. C., & Nagaraja, B. Darcy–Forchheimer flow of dusty tangent hyperbolic fluid over a stretching sheet with Cattaneo-Christov heat flux. *Waves Rand. Comp. Media*. 1–20 (2021).
37. Ramzan, M., Abid, N., Lu, D. & Tlili, I. Impact of melting heat transfer in the time-dependent squeezing nanofluid flow containing carbon nanotubes in a Darcy–Forchheimer porous media with Cattaneo-Christov heat flux. *Comm. Theo. Phy.* **72**(8), 085801 (2020).
38. Jawad, M., Saeed, A., Kumam, P., Shah, Z. & Khan, A. Analysis of boundary layer MHD Darcy–Forchheimer radiative nanofluid flow with Soret and Dufour effects by means of marangoni convection. *Case Stud.* **23**, 100792 (2021).

39. Khan, M. I. Transportation of hybrid nanoparticles in forced convective Darcy–Forchheimer flow by a rotating disk. *Int Com. Heat Mass Tran.* **122**, 105177 (2021).
40. Muhammad, T. *et al.* Significance of Darcy–Forchheimer porous medium in nanofluid through carbon nanotubes. *Comm. Theo. Phys.* **70**(3), 361 (2018).
41. Ramzan, M., Gul, H., & Zahri, M. Darcy–Forchheimer 3D Williamson nanofluid flow with generalized Fourier and Fick's laws in a stratified medium. *Bull. Polish Acad. Sci. Tech. Sci.* **68**(2) (2020).
42. Mehmood, T., Ramzan, M., Howari, F., Kadry, S. & Chu, Y. M. Application of response surface methodology on the nanofluid flow over a rotating disk with autocatalytic chemical reaction and entropy generation optimization. *Sci. Rep.* **11**(1), 1–18 (2021).
43. Ramzan, M., Chung, J. D., Kadry, S., Chu, Y. M. & Akhtar, M. Nanofluid flow containing carbon nanotubes with quartic autocatalytic chemical reaction and Thompson and Troian slip at the boundary. *Sci. Rep.* **10**(1), 1–13 (2020).
44. Khan, M. *et al.* 3-D axisymmetric Carreau nanofluid flow near the Homann stagnation region along with chemical reaction: Application Fourier's and Fick's laws. *Math. Comp. Sim.* **170**, 221–235 (2020).
45. Lu, D. C., Ramzan, M., Bilal, M., Chung, J. D. & Farooq, U. A numerical investigation of 3D MHD rotating flow with binary chemical reaction, activation energy and non-Fourier heat flux. *Comm. Theo. Phys.* **70**(1), 089 (2019).
46. Khan, M., Malik, M. Y., Salahuddin, T. & Khan, F. Generalized diffusion effects on Maxwell nanofluid stagnation point flow over a stretchable sheet with slip conditions and chemical reaction. *J. Braz. Soc. Mech. Sci. Eng.* **41**(3), 1–9 (2019).
47. Ramzan, M., Bilal, M. & Chung, J. D. Numerical simulation of magnetohydrodynamic radiative flow of Casson nanofluid with chemical reaction past a porous media. *Theo. Nanosci.* **14**(12), 5788–5796 (2017).
48. Khan, M., Shahid, A., Malik, M. Y. & Salahuddin, T. Chemical reaction for Carreau-Yasuda nanofluid flow past a nonlinear stretching sheet considering Joule heating. *Res. Phys* **8**, 1124–1130 (2018).
49. Khan, M. *et al.* 3-D axisymmetric Carreau nanofluid flow near the Homann stagnation region along with chemical reaction: application Fourier's and Fick's laws. *Math. Compt. Simul.* **170**, 221–235 (2020).
50. Rehman, K. U., Khan, A. A., Malik, M. Y. & Pradhan, R. K. Combined effects of Joule heating and chemical reaction on non-Newtonian fluid in double stratified medium: A numerical study. *Res. Phys.* **7**, 3487–3496 (2017).
51. Ramzan, M., Gul, H. & Chung, J. D. Double stratified radiative Jeffery magneto nanofluid flow along an inclined stretched cylinder with chemical reaction and slip condition. *Eur. Phys. J. Plus* **132**(11), 1–17 (2017).
52. Lu, D., Ramzan, M., Ahmad, S., Chung, J. D. & Farooq, U. Upshot of binary chemical reaction and activation energy on carbon nanotubes with Cattaneo-Christov heat flux and buoyancy effects. *Phys. Fluids.* **29**(12), 123103 (2017).
53. Sohail, M., Naz, R. & Abdelsalam, S. I. On the onset of entropy generation for a nanofluid with thermal radiation and gyrotactic microorganisms through 3D flows. *Phys. Scr.* **95**(4), 045206 (2020).
54. Khan, M. I., Qayyum, S., Hayat, T., Khan, M. I. & Alsaedi, A. Entropy optimization in flow of Williamson nanofluid in the presence of chemical reaction and Joule heating. *Int. J. Heat Mass Transf.* **133**, 959–967 (2019).
55. Sarojamma, G., Vijaya Lakshmi, R., Satya Narayana, P. V. & Animasaun, I. L. Exploration of the significance of autocatalytic chemical reaction and Cattaneo-Christov heat flux on the dynamics of a micropolar fluid. *J. Appl. Comput. Mech.* **6**(1), 77–89 (2020).
56. Tamoor, M., Waqas, M., Khan, M. I., Alsaedi, A. & Hayat, T. Magnetohydrodynamic flow of Casson fluid over a stretching cylinder. *Res. Phys.* **7**, 498–502 (2017).
57. Yusuf, T. A. & Gbadeyan, J. A. Entropy generation on Maxwell fluid flow past an inclined stretching plate with slip and convective surface conditon: Darcy–Forchheimer model. *NHC.* **26**, 62–83 (2019).
58. Adesanya, S. O., Dairo, O. F., Yusuf, T. A., Onanaye, A. S., & Arekete, S. A. Thermodynamics analysis for a heated gravity-driven hydromagnetic couple stress film with viscous dissipation effects. *Phys. A*. **540**, 123150 (2020).
59. Yusuf, T. A., Adesanya, S. O. & Gbadeyan, J. A. Entropy generation in MHD Williamson nanofluid over a convectively heated stretching plate with chemical reaction. *J. Heat Transfer.* **49**(4), 1982–1999 (2020).
60. Mabood, F., Yusuf, T. A., & Sarris, I. E. Entropy generation and irreversibility analysis on free convective unsteady MHD Casson fluid flow over a stretching sheet with Soret/Dufour in porous media. *Int. J.* **11**(6), (2020).
61. Mabood, F., Yusuf, T. A., & Khan, W. A. (2021). Cu–Al_2 O_3–H_2O hybrid nanofluid flow with melting heat transfer, irreversibility analysis and nonlinear thermal radiation. *J. Therm. Anal. Calorim.* **143**(2), 973–984 (2021).
62. Mabood, F., Yusuf, T. A., & Bognár, G. Features of entropy optimization on MHD couple stress nanofluid slip flow with melting heat transfer and nonlinear thermal radiation. *Sci. Rep*. **10**(1), 1–13 (2020).
63. Mabood, F., Yusuf, T. A., Rashad, A. M., Khan, W. A. & Nabwey, H. A. Effects of combined heat and mass transfer on entropy generation due to MHD nanofluid flow over a rotating frame. *CMC.* **66**(1), 575–587 (2021).
64. Yusuf, T. A., Mabood, F., Khan, W. A. & Gbadeyan, J. A. Irreversibility analysis of Cu-TiO_2-H_2O hybrid-nanofluid impinging on a 3-D stretching sheet in a porous medium with nonlinear radiation: Darcy–Forchhiemer's model. *Alex. Eng. J.* **59**, 5247–5261 (2020).
65. Almeida, F., Gireesha, B. J., Venkatesh, P., & Ramesh, G. K. Intrinsic irreversibility of Al_2O_3–H_2O nanofluid Poiseuille flow with variable viscosity and convective cooling. *Int. J. Numer. Method H.* (2020).
66. Hayat, T., Rashid, M., Alsaedi, A. & Asghar, S. Nonlinear convective flow of Maxwell nanofluid past a stretching cylinder with thermal radiation and chemical reaction. *J. Braz. Soc. Mech. Sci. Eng.* **41**(2), 86 (2019).
67. Raju, C. S. K. *et al.* The flow of magnetohydrodynamic Maxwell nanofluid over a cylinder with Cattaneo-Christov heat flux model. *Cont. Mech. Thermodyn.* **29**(6), 1347–1363 (2017).
68. Khan, J. A. & Mustafa, M. A numerical analysis for non-linear radiation in MHD flow around a cylindrical surface with chemically reactive species. *Res. Phys.* **8**, 963–970 (2018).

Acknowledgements

The authors extend their appreciation to the Deanship of Scientific Research at King Khalid University, Abha 61413, Saudi Arabia for funding this work through research groups program under Grant number RGP-1-96-42.

Author contributions

M.R. did conceptualization, M.U.K. worked on methodology, C.L. did validation and formal analysis, Y.M.C. wrote the original draft, S.K., and C.L. worked on software. Y.M.C. arranged the funds, M.Y.M and R.C. helped in the revised draft and partial funding arrangements.

Funding

The research was supported by the National Natural Science Foundation of China (Grant Nos. 11971142, 11871202, 61673169, 11701176, 11626101, 11601485).

Competing interests

The authors declare no competing interests.

Additional information

Correspondence and requests for materials should be addressed to Y.-M.C.

Reprints and permissions information is available at www.nature.com/reprints.

Publisher's note Springer Nature remains neutral with regard to jurisdictional claims in published maps and institutional affiliations.